Volume 3
Number 8
August 2025
Pages 3217–3616

RSC Sustainability

rsc.li/rscsus

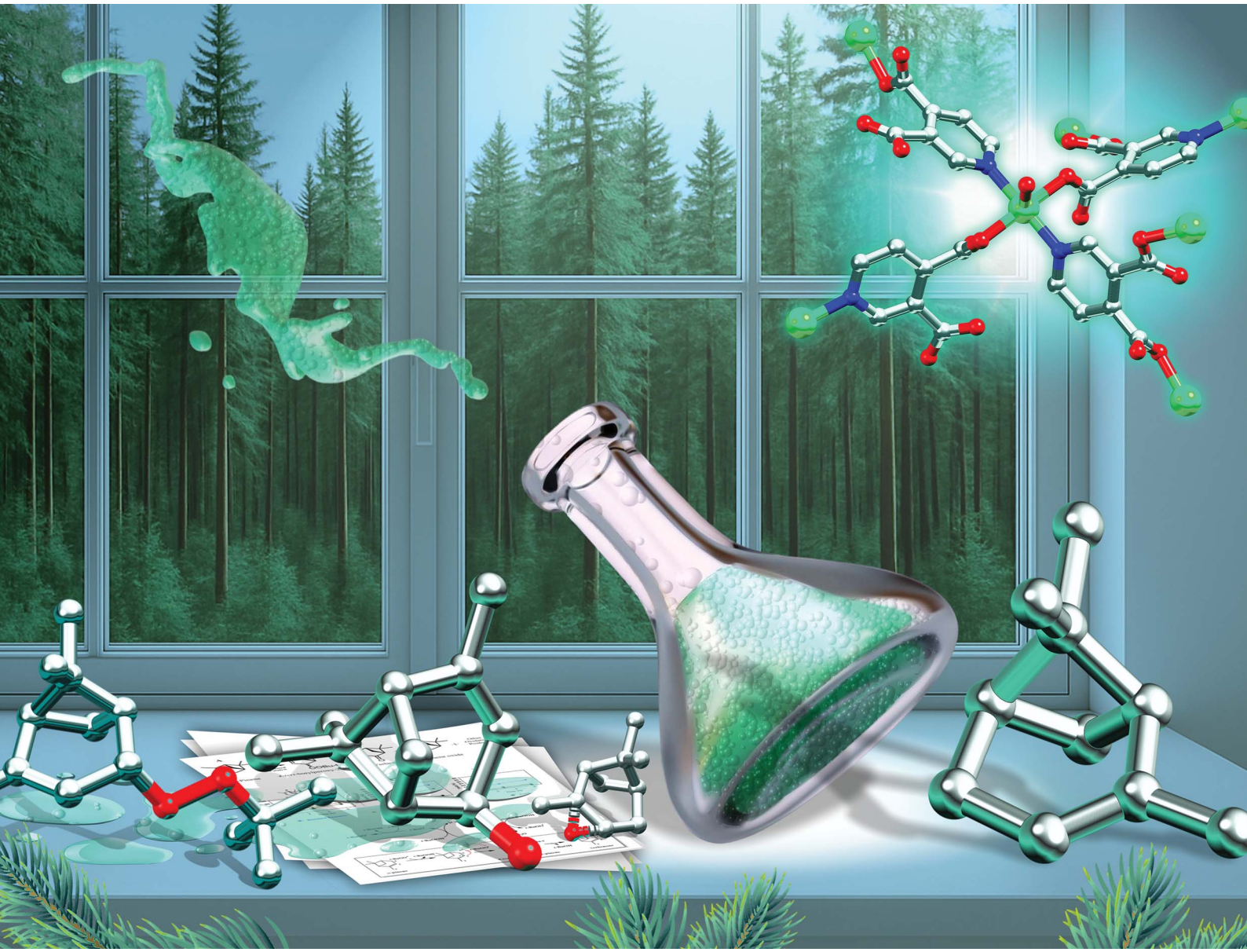

ISSN 2753-8125

ROYAL SOCIETY OF CHEMISTRY

PAPER
Alexander M. Kirillov *et al.*
From α-pinene feedstock to value-added products: scalable and recyclable copper(II) catalysts for allylic oxidation

RSC Sustainability

ROYAL SOCIETY OF CHEMISTRY

PAPER

View Article Online
View Journal | View Issue

Cite this: *RSC Sustainability*, 2025, **3**, 3396

From α-pinene feedstock to value-added products: scalable and recyclable copper(II) catalysts for allylic oxidation†

Gilvan A. Correia, [a] Chris H. J. Franco, [a] Marina V. Kirillova, [a] Alexandre Pradal, [b] Giovanni Poli, [b] Fabrice Gallou [c] and Alexander M. Kirillov *[a]

α-Pinene is one of the most abundant and low-cost terpenes that can be used as an attractive and renewable feedstock for generating added-value products *via* allylic oxidation. Aiming to develop more sustainable catalytic materials for the functionalization of terpenes, in this work two new 2D coordination polymers (CPs), $\{[Cu_2(\mu\text{-pdc})(\mu_3\text{-pdc})(H_2mdea)(H_2O)_2]\cdot 2H_2O\}_n$ (**Cu-mdea**) and $\{[Cu_2(\mu\text{-pdc})(\mu_3\text{-pdc})(H_3tipa)(H_2O)_2]\cdot 4H_2O\}_n$ (**Cu-tipa**) (H_2pdc = 3,4-pyridinedicarboxylic acid, H_2mdea = *N*-methyldiethanolamine and H_3tipa = triisopropanolamine) were synthesized *via* a self-assembly method under green conditions. These compounds were obtained from low-cost and environmentally tolerable reagents, and their scale-up process was also optimized in a 'crystalline reactor' from the milligram to gram scale. The obtained CPs were applied as efficient and recyclable heterogeneous catalysts for the mild oxidation of α-pinene. The effects of various reaction parameters, temperature-dependent and mechanistic features, and catalyst stability were investigated in detail, leading to up to 93% of α-pinene conversion with good yields of 4-*tert*-butylperoxy-2-pinene (42%) and verbenone (25%) as main oxidation products. This study extends the application of α-pinene as a renewable feedstock for the synthesis of value-added oxidation products using recyclable heterogeneous catalysts and mild reaction conditions.

Received 6th January 2025
Accepted 17th May 2025

DOI: 10.1039/d5su00009b

rsc.li/rscsus

Sustainability spotlight

The sustainability approach of the present work is addressed through the use of cost-efficient and recyclable heterogeneous catalysts, the exploration of α-pinene as a highly abundant and renewable substrate for added-value oxidation products, and the reaction process under mild conditions. This research aligns with several of the United Nations Sustainable Development Goals (SDGs), particularly those focused on responsible consumption and production (SDG 12), industry innovation and infrastructure (SDG 9), and climate action (SDG 13). This study showcases how sustainable, noble metal-free catalytic systems can deliver high performance, while addressing challenges in chemical transformations of renewable feedstocks.

Introduction

Transition-metal-catalyzed allylic oxidation is recognized as a powerful strategy for a variety of precursors that are important target molecules in the pharmaceutical and fragrance industries.[1,2] Allylic oxidation of alkenes is an excellent example of C–H bond activation with substantial synthetic importance.[3] The most common catalysts and/or cocatalysts employed in such transformations are based on copper,[4] selenium,[5,6] rhodium,[7] and palladium[8–11] systems. In particular, the latter was extensively employed in the industry to achieve different depths of alkene oxidation, including the incorporation of oxygenated functional groups at the allylic position.[12,13] Due to elevated cost, low turnover numbers and toxicity of noble metals,[3] there is a constant need for new catalytic materials and methodologies based on the use of more affordable, abundant and environmentally tolerable first-row transition metals.[14–16]

Copper-based catalysis has emerged as a sustainable alternative for many reactions, including oxidative transformations.[17–22] Copper catalysts may provide significant benefits, such as low cost and toxicity, in addition to interesting selectivity and attractive substrate scope.[17] Besides, there is

[a]*MINDlab: Molecular Design & Innovation Laboratory, Centro de Química Estrutural, Institute of Molecular Sciences, Departamento de Engenharia Química, Instituto Superior Técnico, Universidade de Lisboa, Av. Rovisco Pais, 1049-001, Lisboa, Portugal. E-mail: kirillov@tecnico.ulisboa.pt*

[b]*Sorbonne Université, Faculté des Sciences et Ingénierie, CNRS, Institut Parisien de Chimie Moléculaire, IPCM, 4 Place Jussieu, 75005 Paris, France*

[c]*Chemical & Analytical Development, Novartis Pharma AG, 4056, Basel, Switzerland*

† Electronic supplementary information (ESI) available: Additional data on the synthesis, characterization, and catalytic application of **Cu-mdea** and **Cu-tipa** (Schemes S1 and S2, Fig. S1–S30, and Tables S1–S14). CCDC 2381054 and 2381055. For ESI and crystallographic data in CIF or other electronic format see DOI: **https://doi.org/10.1039/d5su00009b**

a plethora of copper-containing enzymes with a recognized oxidation function (*e.g.*, particulate methane monooxygenase, multicopper oxidases), which can activate molecular oxygen to generate a selective high-valence oxidizing species, thus motivating the design of biomimetic copper-based coordination compounds as catalysts for the oxidation of various substrates.[23–31] Copper(II) coordination polymers (CPs) may also act as heterogeneous catalysts with potential for recyclability.[20,29,31–33] The most common approach to generate CPs employs carboxylic acids as building blocks, which ensure charge balance and versatile bridging modes within the coordination polymer structure.[34–37]

With regard to substrates for allylic oxidation, nature provides a fascinating set of cheap, abundant, and renewable raw materials known as terpenes.[38–40] These molecules serve as versatile substrates for organic synthesis, owing to their wide-range applications as intermediates in the pharmaceutical, perfume, and fragrance industries.[15] Specifically, α-pinene is one of the most abundant terpenes available from many coniferous trees and essential oils.[41] It possesses a relatively simple structure and well-understood reactivity, thus being an attractive model substrate for investigating novel catalytic systems in oxidation reactions, including the allylic oxidation of terpenes.[41]

Considering the above discussion and our interest in developing copper(II) catalytic systems for the mild oxidation of hydrocarbons, the primary research objectives of the present work were: (1) to design and assemble new copper(II) CPs from a multicomponent reaction system composed of Cu^{2+} ions, amino alcohol chelators,[29,42–44] and 3,4-pyridinedicarboxylic acid (H_2pdc) linkers, and (2) to evaluate the catalytic behavior of the obtained CPs as heterogeneous catalysts in the allylic oxidation of α-pinene. As amino alcohol chelators, *N*-methyldiethanolamine (H_2mdea) and triisopropanolamine (H_3tipa) were explored on account of their low cost, aqueous solubility, and recognized chelating and structure-stabilizing behavior toward copper(II) ions.[45–48] The selection of H_2pdc was governed by the presence of two types of donor atoms (N,O) and its relatively underexplored use for the design of CPs.[49,50] In addition, such N-heterocyclic carboxylic acids and derived ligands may also promote the oxidation of hydrocarbons.[51]

Thus, we describe herein the syntheses, scale-up process, full characterization, and crystal structures, as well as a detailed catalytic investigation of two new copper(II) 2D coordination polymers $\{[Cu_2(\mu\text{-pdc})(\mu_3\text{-pdc})(H_2mdea)(H_2O)_2]\cdot 2H_2O\}_n$ (**Cu-mdea**) and $\{[Cu_2(\mu\text{-pdc})(\mu_3\text{-pdc})(H_3tipa)(H_2O)_2]\cdot 4H_2O\}_n$ (**Cu-tipa**). These CPs were easily assembled in a water/ethanol medium and applied as effective heterogeneous catalysts for the oxidation of α-pinene into value-added products, which include 4-*tert*-butylperoxy-2-pinene and verbenone.

Experimental

General synthetic procedure for Cu-mdea and Cu-tipa

3,4-Pyridinedicarboxylic acid (3,4-H_2pdc, 0.5 mmol, 83 mg) was dissolved in ethanol (7 mL), followed by the addition of aqueous NH_4OH (4 mmol, 1 mL, 4 M) to produce the reaction solution A (Fig. 1). In parallel, an aqueous solution of $Cu(NO_3)_2\cdot 3H_2O$ (1.2 mmol, 1.2 mL, 1 M) was mixed with *N*-methyldiethanolamine (H_2mdea, 1 mmol, 119 mg) or triisopropanolamine (H_3tipa, 1 mmol, 191 mg) under stirring in air at 80 °C, producing the reaction solution B. Then, the reaction solution B was slowly added into A under constant stirring at 80 °C to give rise to mixture C. This was stirred for an additional 30 min, then filtered and refluxed for 1 h. Finally, the reaction mixture was transferred to an open glass vial that was kept for slow evaporation in the air. Blue crystals were formed in a week after partial evaporation of the filtrate, collected manually, and dried in air at room temperature to give **Cu-mdea** and **Cu-tipa** in 65 and 60% yields based on copper(II) nitrate, respectively. Analytical data: $\{[Cu_2(\mu\text{-pdc})(\mu_3\text{-pdc})(H_2mdea)(H_2O)_2]\cdot 2H_2O\}_n$ (**Cu-mdea**), calculated for $Cu_2C_{19}H_{27}N_3O_{14} + H_2O$ (MW 666.5): C, 34.24%; H, 4.39%; N, 6.30%; found: C, 34.16%; H, 4.12%; N, 7.06%. FTIR-ATR (cm^{-1}): 3268 (s br) ν(OH/H_2O), 2108 (w) ν(CH), 1937 (w), 1617 (s) ν as(COO), 1598 (m), 1483 (w) ν s(COO), 1365 (s), 1193 (w), 1166 (w), 1119 (m), 1076 (m), 1060 (w), 1019 (w), 994 (w), 957 (w), 879 (w), 840 (w), 781 (s), 727 (s) and 683 (s). $\{[Cu_2(\mu\text{-pdc})(\mu_3\text{-pdc})(H_3tipa)(H_2O)_2]\cdot 4H_2O\}_n$ (**Cu-tipa**), calculated for $Cu_2C_{23}H_{39}N_3O_{17} + H_2O$ (MW 774.7): C, 35.65%; H, 5.33%; N, 5.42%; found: C, 35.61%; H, 4.66%; N, 6.07%. FTIR-ATR (cm^{-1}): 3396 (s br) ν(OH/H_2O), 2975 (w) ν(CH), 2975 (w), 1627 (s) ν as(COO), 1585 (m), 1553 (m), 1483 (w) ν s(COO), 1382 (s), 1122 (w), 970 (m), 837 (w), 781 (w), 729 (w) and 683 (w). Additional characterization details are given in ESI Fig. S1–S7.†

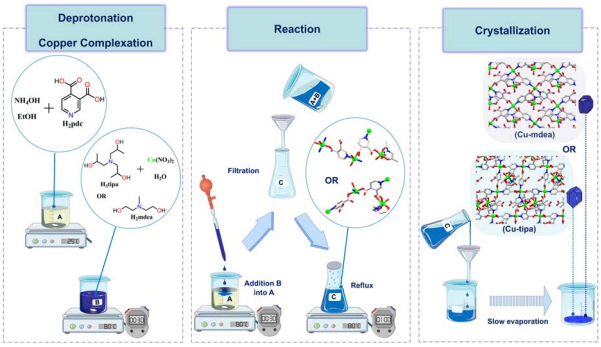

Fig. 1 Synthesis of **Cu-mdea** and **Cu-tipa** in an aqueous ethanol medium.

Scale-up procedure for Cu-mdea and Cu-tipa

In a round-bottom flask, H_2pdc (4.1 g, 25 mmol), water (100 mL), and aqueous NH_4OH (100 mmol, 25 mL, 4 M) were combined to produce the reaction solution A, which was then stirred for 0.5 h at room temperature. In another flask, $Cu(NO_3)_2\cdot 3H_2O$ (11.3 g, 47 mmol) was mixed with H_2mdea (47 mmol, 5.6 g) or H_3tipa (47 mmol, 9.0 g) in ethanol (100 mL) for 0.5 h at 80 °C to give the reaction solution B. Afterwards, the solutions A and B were mixed in a 300 mL Lab Reactor FlexyCUBE from SYSTAG, for 3 h at 80 °C. The real-time monitoring of the reactor ensured that the parameters were stable over the reaction time (pH 8–9; pressure 0.98–1.23 bar; reflux cooler: 5 °C; glass anchor stirrer: 300 rpm). Finally, the reaction mixture was filtered and split into twelve Falcon tubes. They were left to

rest in a reflux system at 80 °C for 3 h. As a result, blue crystalline samples of **Cu-mdea** and **Cu-tipa** were instantly formed. To achieve higher yields, the Falcon tubes were opened and left to slowly evaporate at room temperature for one week. For details, see the diagram in Fig. S11 (ESI).† The above-mentioned optimized conditions were initially established by self-assembly synthesis, then confirmed through iterative experimentation using 10 mL vessels in a 'crystalline reactor' (Crystalline – Technobis Crystallization Systems) and finally tested in a 300 mL Lab Reactor. These scale-up conditions were successfully reapplied using a 500 mL round-bottom flask instead of Lab Reactor, demonstrating that the procedure is easily accessible and may be performed without using specialized equipment or precise parameters. The pivotal step in the procedure is to split the filtered reaction mixture and keep it without stirring under near reflux conditions (80 °C, 3 h).

Single-crystal X-ray diffraction

For **Cu-mdea**, a blue block-shaped crystal with the dimensions of $0.12 \times 0.10 \times 0.08$ mm^3 was selected for collecting the X-ray data on a Bruker APEX-II CCD diffractometer at 298 K. Data were measured using Mo Kα radiation ($\lambda = 0.71073$ Å). For **Cu-tipa**, a dark blue block-shaped crystal with the dimensions of $0.11 \times 0.08 \times 0.05$ mm^3 was mounted and data were collected using a Bruker D8 Venture, dual, Photon II diffractometer at 150 K and a Mo Kα radiation ($\lambda = 0.71073$ Å). Data reduction, scaling and absorption corrections were performed using SAINT V8.40B,[52] for both **Cu-mdea** and **Cu-tipa**. The structure of **Cu-mdea** was solved with the ShelXS 2018/2 (ref. 53) program using iterative methods and Olex2 as the graphical interface.[54] For **Cu-tipa**, a multi-scan absorption correction was performed using TWINABS-2012/1,[55] followed by structure solution by the ShelXS[56] using direct methods. Both crystal structures were refined with ShelXL 2018/3 (ref. 57) using full matrix least squares minimisation on F^2. All non-hydrogen atoms were refined anisotropically. Most hydrogen atom positions were calculated geometrically (C–H = 0.87–0.98 Å) and refined using the riding model with $U_{iso}(H) = 1.2U_{eq}(C)$ or $1.5U_{eq}(C)$ for H atoms bonded to oxygen atoms. The structure of **Cu-tipa** was refined as a 2-component twin [BASF 0.143(2)]. CCDC codes 2381054 and 2381055.

Powder X-ray diffraction

Powder X-ray diffraction data for the compounds were obtained using a D8 Advance diffractometer with Cu Kα ($\lambda = 1.54056$ Å), operating at 40 kV and 30 mA, with a Ni filter and a LynxEye linear detector. The diffractograms were collected in the 2θ angular range from 5 to 50°, with a typical step size of 0.02°, and counting time ranging from 0.5 to 1 s per step with a divergence slit of 0.6 mm and primary/secondary Soller slits of 2.5°. A comparison of simulated and experimental diffractograms confirmed the purity of the as-prepared microcrystalline products (Fig. S4 and S7, ESI†).

General procedure for oxidation of α-pinene

A Cu-based catalyst (0.5 to 3 mol% of solid catalyst *vs.* substrate) and a solution of α-pinene (96 μL, 0.6 mmol) in CH_3CN (1 mL) were combined in a 2 mL catalytic flask, equipped with an 11 mm stirring bar. Subsequently, TBHP (70% in H_2O, 167 μL, 1.2 mmol) was introduced. The catalytic flask was sealed, and the reaction medium was stirred at 1200 rpm for 5–12 h at 60 °C. Nitromethane (71 μL, 1.32 mmol) was used as an internal gas chromatography standard and introduced into the initial reaction mixture to monitor the reaction progress. Small aliquots were withdrawn and analyzed *via* gas chromatography (GC). Before collecting aliquots, the reaction mixture was allowed to rest for 3–5 min to ensure that the catalyst settled to the bottom of the vial. At the end of the reaction, the resulting solution was centrifuged at 7000 rpm for 2 min to separate the catalyst. Finally, the catalyst was washed with ethanol three times, left to slowly dry at room temperature for 24 h, and reused in the next run. For further details on the catalytic experiments, see the ESI.†

Results and discussion

Synthesis, scale-up, and characterization of Cu-mdea and Cu-tipa

The 2D coordination polymers $\{[Cu_2(\mu\text{-pdc})(\mu_3\text{-pdc})(H_2\text{-mdea})(H_2O)_2]\cdot 2H_2O\}_n$ (**Cu-mdea**) and $\{[Cu_2(\mu\text{-pdc})(\mu_3\text{-pdc})(H_3\text{-tipa})(H_2O)_2]\cdot 4H_2O\}_n$ (**Cu-tipa**) were assembled by reacting copper(II) nitrate with the corresponding amino alcohol chelators (H_2mdea or H_3tipa) and H_2pdc as a linker. The syntheses were performed in water–ethanol medium at 80 °C. To control the pH (up to 9) of the reaction mixture, an aqueous NH_4OH solution was used. The crystal structures of the obtained compounds were determined by single-crystal X-ray diffraction and further confirmed by standard methods, including FTIR spectroscopy, elemental and thermal analyses, and powder X-ray diffraction.

With an objective to scale-up the synthesis process from a milligram to gram scale, the reactions were carried out in a 'crystalline reactor'. The quantities of the starting materials were increased proportionally, and the reaction parameters remained similar to those employed in the small-scale model reaction. The success of the scale-up process depended on splitting the reaction medium into different Falcon tubes and subjecting them to a reflux system at 80 °C without stirring. Over the next several hours, a blue crystalline powder formed on the walls of the Falcon tubes. This process yielded a significant amount of products (~8 g scale, Fig. S11, ESI†). The main advantages of these findings include the consistent reproducibility of the syntheses of these two copper CPs on a larger scale. This scale-up process is robust and can be easily adapted for the synthesis of similar CPs. In a separate attempt, the reaction solution was left to reflux in a large reaction vessel. However, no crystals were obtained, emphasizing the importance of splitting the solution into smaller flasks for reflux to achieve good yields and synthetic reproducibility.

In fact, the optimized scale-up process resulted in higher yields of **Cu-mdea** (69%) and **Cu-tipa** (74%) when compared to a mg-scale self-assembly reaction (60%). Additionally, the similarity in PXRD patterns of the samples obtained by different

methods confirmed that both compounds retain their pure crystalline phases (Fig. S12 and S13, ESI†).

FTIR spectroscopic data of **Cu-mdea** and **Cu-tipa** show broad absorption bands with maxima at 3268 and 3396 cm^{-1} (Fig. S2 and S5, ESI†) that correspond to $\nu(OH/H_2O)$ vibrations of hydroxyl groups in amino alcohol ligands and water moieties. The $\nu(C{=}N)_{py}$ bands are observed at 1598 and 1594 cm^{-1} for **Cu-mdea** and **Cu-tipa**, respectively. When compared to a free H_2pdc ligand (1641 cm^{-1}), these bands are shifted to lower wavenumbers, which is indicative of N_{py} coordination to the copper(II) center. Furthermore, strong absorptions with maxima at 1617 and 1365 cm^{-1} for **Cu-mdea** and 1627 and 1385 cm^{-1} for **Cu-tipa** are attributed to $\nu_{as}(COO^-)$ and $\nu_s(COO^-)$ bands, respectively.[58] These bands also support a deprotonated nature of pdc^{2-} ligands, which agrees with the X-ray crystallographic data.

Thermogravimetric analyses of both compounds (Fig. S3 and S6, ESI†) indicate three major mass loss events. The first one at 100–130 °C corresponds to a release of all water molecules, with the mass loss of 12.1% (calcd 12.6%) for **Cu-mdea** and 13.2% (calcd 13.4%) for **Cu-tipa**. Further thermal effects refer to the gradual thermal-decomposition of the samples that starts at ~190–200 °C and is essentially complete at ~380–400 °C, resulting in the formation of 2CuO (sample remaining weight: exp. 22.5%, calcd 22.2% for **Cu-mdea**; exp. 21.0%, calcd 21.3% for **Cu-tipa**).

Structural description

The compounds **Cu-mdea** and **Cu-tipa** are 2D coordination polymers, which crystallize in the centrosymmetric monoclinic system with the $P2_1/c$ and $C2/c$ space groups, respectively. X-ray crystallographic details are summarized in Table 1, while the selected geometric parameters are listed in Tables S1–S4 (ESI).† Both CPs possess two types of copper(II) centers, two distinct μ-pdc^{2-} and μ_3-pdc^{2-} linkers and one neutral amino alcohol ligand (Fig. 2). In **Cu-mdea**, the 'central' 5-coordinated Cu(II) atom adopts an almost ideal square pyramidal $\{CuO_3N_2\}$ geometry ($\tau_5 = 0.04$).[59] In equatorial positions, there are two oxygen and two nitrogen atoms from the bridging pdc^{2-} ligands, whereas the water ligand occupies an axial position. The second Cu(II) atom adopts a distorted square pyramidal $\{CuO_4N\}$ environment ($\tau_5 = 0.27$),[59] which is taken by two O and one N donors of H_2mdea, along with a carboxylate oxygen from pdc^{2-} and a water ligand. Similar to what is observed in **Cu-mdea**, the 'central' 5-coordinated Cu(II) atom in **Cu-tipa** shows almost an ideal square pyramidal $\{CuO_3N_2\}$ environment ($\tau_5 =$ 0.07 for Cu1 and $\tau_5 = 0.01$ for Cu3). The coordination distances between Cu–O (1.97–2.41 Å) and Cu–N (~2.00 Å) are within the range expected for related structures.[49] Besides, the Cu2 center with a $\{CuO_4N\}$ environment in the crystal structure of **Cu-tipa** is also 5-coordinated by H_3tipa and a water ligand (equatorial position), and displays an almost ideal square pyramidal geometry ($\tau_5 = 0.05$ for Cu2). In both structures, each of the "central" copper units, $\{CuO_3N_2\}$, is cross-linked to four adjacent units *via* the pdc^{2-} moieties, thus leading to 2D coordination polymer structures with square-like voids of 8.9 × 8.9 Å dimensions (Fig. 3). From a topological perspective, the crystal structures can be defined as an uninodal 4-connected net with a $(4^4.6^2)$ point symbol, which corresponds to an sql (Shubnikov tetragonal plane net) topology.[60,61] The potential open windows

Table 1 Crystal data and structure refinement details for **Cu-mdea** and **Cu-tipa**

Compound	**Cu-mdea**	**Cu-tipa**
Formula	$\{[Cu_2(\mu\text{-pdc})(\mu_3\text{-pdc})(H_2mdea)(H_2O)_2]\cdot 2H_2O\}_n$	$\{[Cu_2(\mu\text{-pdc})(\mu_3\text{-pdc})(H_3tipa)(H_2O)_2]\cdot {}_4H_2O\}_n$
$D_{calc.}$/g cm^{-3}	1.705	1.611
μ/mm^{-1}	1.758	1.446
Formula weight	648.51	755.64
Size/mm^3	0.12 × 0.10 × 0.08	0.11 × 0.08 × 0.05
Crystal system	Monoclinic	Monoclinic
Space group	$P2_1/c$	$C2/c$
a/Å	13.9122(6)	17.6112(11)
b/Å	10.8868(4)	20.3103(11)
c/Å	16.8263(7)	17.6199(11)
α/°	90	90
β/°	97.444(2)	98.672(3)
γ/°	90	90
V/$Å^3$	2527.02(18)	6230.4(6)
Z	4	8
Radiation type	Mo Kα	Mo Kα
Measured Refl's	49 574	172 915
Indep't Refl's	4615	5795
Refl's I ≥ 2 s(I)	4087	5052
Rint	0.0367	0.0879
Parameters	328	435
Restraints	6	5
GooF	1.044	1.043
wR2	0.1678	0.1884
R1	0.0589	0.0632

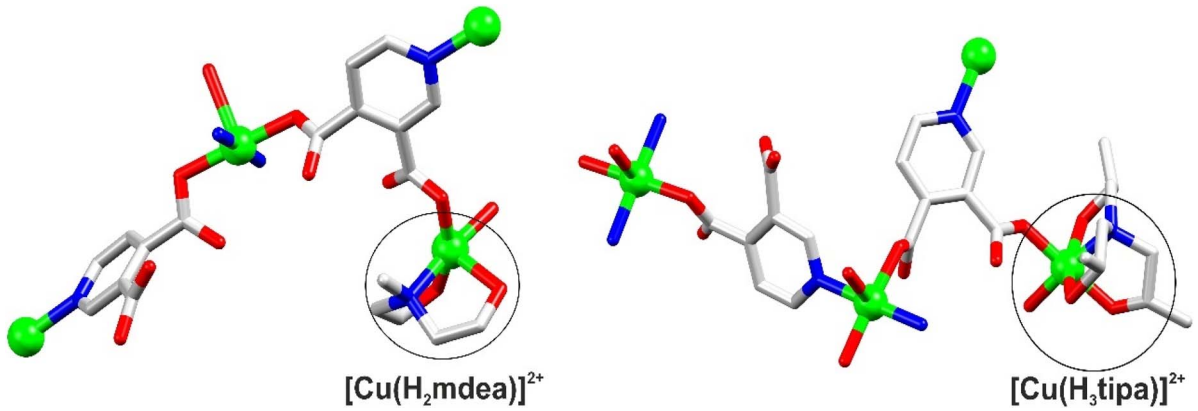

Fig. 2 Crystal structure fragments of **Cu-mdea** (left) and **Cu-tipa** (right). Color codes: Cu green balls, O red, N blue, C gray. H atoms and solvent molecules were excluded for clarity.

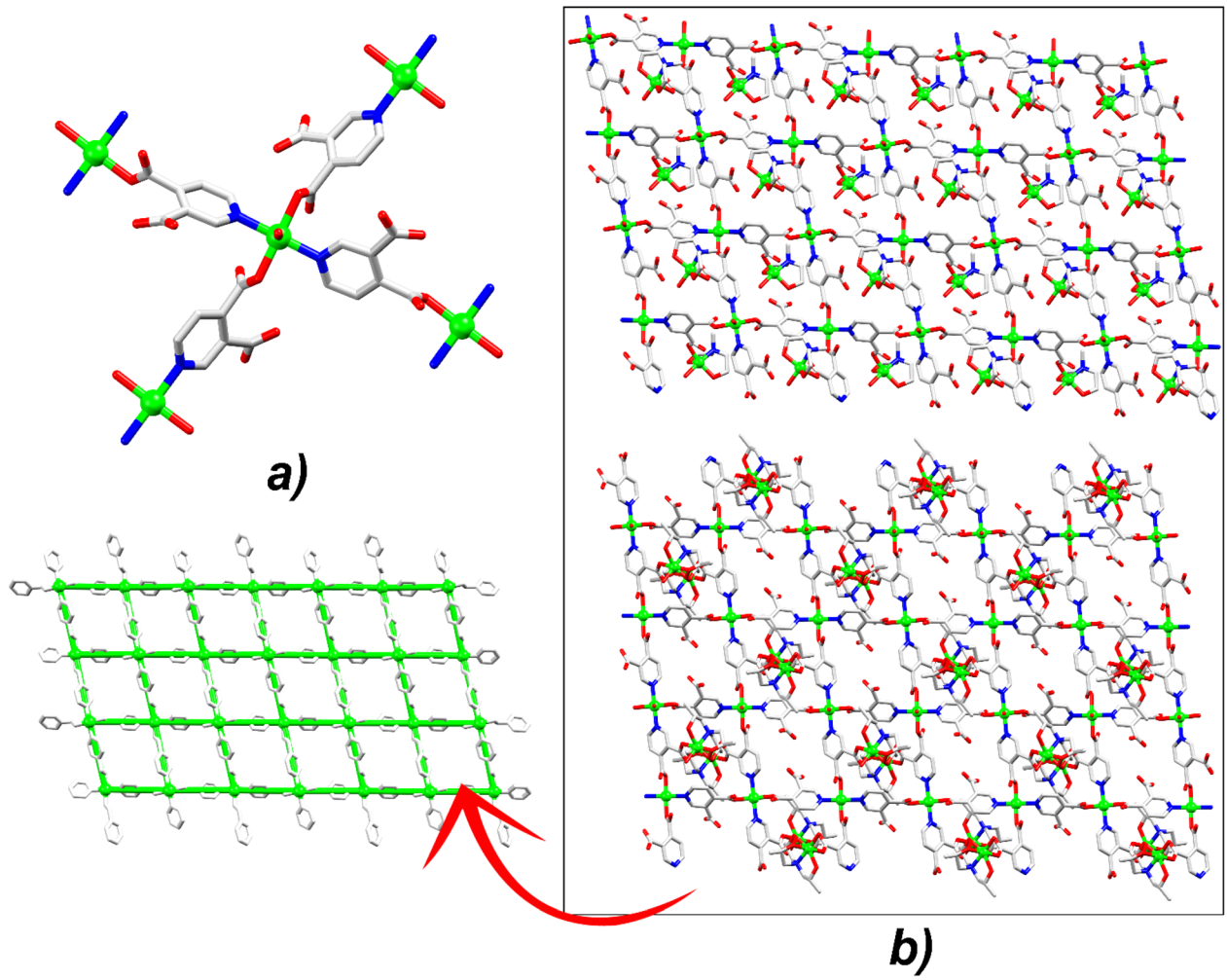

Fig. 3 (a) Illustration of 'central' $\{CuO_3N_2\}$ blocks interconnected by four adjacent square pyramidal units through pdc^{2-} linkers in **Cu-tipa** (similar interconnections are seen in **Cu-mdea**, top). Color codes: Cu green balls, O red, N blue, C gray. (b) 2D metal–organic layers formed in **Cu-mdea** (top) and **Cu-tipa** (bottom) directed by the $\{CuO_3N_2\}$ units. Topological representation of the simplified uninodal 4-connected underlying net with the sql topology; green balls are the centroids of the $\{CuO_3N_2\}$ units.

are blocked due to the intercalated arrangement of the crystalline packing in the 2D layers and the positioning of the $[Cu(aminoalcohol)]^{2+}$ units at the center of the square windows (Fig. S9 and S10, ESI†). Despite this, both compounds may endow materials with bulk mesoporous properties.[62,63] Although neither H_2mdea nor H_3tipa contributes to the

network topology, their incorporation plays a structure-stabilizing role.

Catalytic oxidation of α-pinene

Oxidation of α-pinene (Scheme 1) is a good model to investigate allylic oxidation reactions catalyzed by copper(II) coordination polymers, owing to the abundance, low cost, and, most importantly, structure of this substrate.[64]

To determine the optimal conditions for α-pinene oxidation, a screening of many variables was investigated in this catalytic study, including temperature, solvent, substrate, oxidant, and catalyst loading. Initially, several commercial oxidants [*tert*-butyl hydroperoxide (TBHP), 70% in H_2O; H_2O_2, 50% in H_2O, *tert*-butyl peroxybenzoate (TBPB); *m*-chloroperoxybenzoic acid (*m*-CPBA); and peracetic acid (CH_3COOOH), 50% in H_2O] were screened alongside **Cu-mdea** as a catalyst to identify the most effective oxidant for this type of catalytic system. The reactions were run in an aqueous acetonitrile medium, and a summary of the results is presented in Table 2. A typical chromatogram of the reaction mixture in the α-pinene oxidation is given in Fig. S15 (ESI).†

As a result, a noticeable increase in the conversion of α-pinene was achieved using TBHP (89% conversion), H_2O_2 (97%), and *m*-CPBA (97%) as oxidants after 9 h (Table 2, entries 1, 2, and 4). In contrast, a moderate conversion was observed when the same reaction is carried out with TBPB and peracetic acid (64 and 41% conversion, respectively; Table 2, entries 3 and 5). Although the reactions with H_2O_2 (1 h) and *m*-CPBA (9 h) led to the highest conversion values in this study, low product selectivity and catalyst degradation pose challenges for the application of these systems in the allylic oxidation reactions. These non-selective reactions can be explained either by the reactivity order at an α-position (CH > CH_2 > CH_3), in which the abstraction of an H atom favors the formation of diverse resonance-stabilized species, resulting in different products, such as 4-*tert*-butylperoxy-2-pinene, verbenol and verbenone; or *via* a transition-metal-catalyzed epoxidation of a double-bond, giving rise to pinanediol and α-campholenal (Scheme S1, ESI†).[24,65]

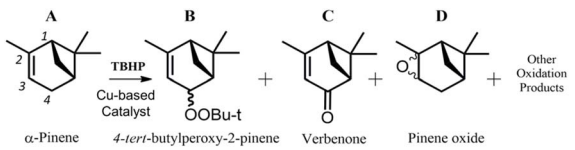

Scheme 1 Cu-catalyzed oxidation of α-pinene ((A) α-pinene, (B) 4-*tert*-butylperoxy-2-pinene, (C) verbenone, (D) pinene oxide).

Based on these preliminary studies, TBHP was selected as an oxidant due to its reactivity and tolerance toward the catalyst, thus facilitating its recovery. This assumption is consistent with prior studies on the Cu-catalyzed allylic oxidation with TBHP.[66] Moreover, the optimal molar ratio of oxidant-to-pinene in the oxidation reaction using CH_3CN as the solvent was determined to be 2 : 1, with no significant variations compared to the molar ratio of 3 : 1 (Table S5, ESI†). The gradual addition of TBHP also did not imply any influence on the oxidation reaction (Fig. S16, ESI†).

Since **Cu-mdea** and **Cu-tipa** possess isoreticular coordination networks, it was expected that their catalytic activities might be similar. Indeed, both 2D CPs exhibited comparable catalytic behavior in the allylic oxidation of α-pinene at 60 °C (Fig. 4), resulting in the maximum substrate conversion of 90–92%, with the formation of 4-*tert*-butylperoxy-2-pinene (31%, Fig. 4B) and verbenone (13.5%, Fig. 4C) as main products after 12 h. The formation of alkyl *tert*-butyl peroxide as the primary reaction product is particularly interesting, given its status as a highly reactive intermediate with potential application in organic synthesis.[67] In contrast, in the absence of catalyst (blank test), there is no significant conversion of α-pinene (25.5% conversion after 12 h), reaching a total 6.5% yield of the main products (Table S6, ESI†).

Furthermore, to enhance our comprehension of the α-pinene oxidation reaction, an investigation was conducted involving variations of protic and aprotic solvents, using TBHP as the oxidant. Hence, acetonitrile, ethyl acetate, acetone, DMSO, propan-2-ol and THF were screened with **Cu-mdea** as

Table 2 Oxidation of α-pinene with different oxidants catalyzed by **Cu-mdea**

Entry	Oxidant	Oxidant-to-substrate molar ratio[a]	Conversion (%)[c] 1 h	9 h	Main identified products[b]
1	TBHP, 70% in H_2O	2	59.0	89.0	4-*tert*-Butylperoxy-2-pinene and verbenone
2	H_2O_2, 50% in H_2O	3	94.0	97.0	Catalyst decomposition[b]
3	TBPB	3	56.0	64.0	Partial oxidation of solvent and catalyst decomposition[b]
4	*m*-CPBA	2	—	97.0	Epoxide derivatives (diols, verbenone, α-campholenal)[b]
5	CH_3COOOH, 50% in H2O	3	30.5	41.0	Epoxide derivatives (diols, α-campholenal)[b]

[a] Conditions: α-pinene (0.6 mmol), **Cu-mdea** (1 mol%), oxidant (1.2–1.8 mmol), CH_3CN (1 mL), 1–9 h, 1200 rpm, 60 °C, catalytic flask (2 mL). [b] Traces of these products were identified by GC-MS. [c] Conversion: [moles of initial α-pinene – moles of final α-pinene/(moles of initial α-pinene) × 100%].

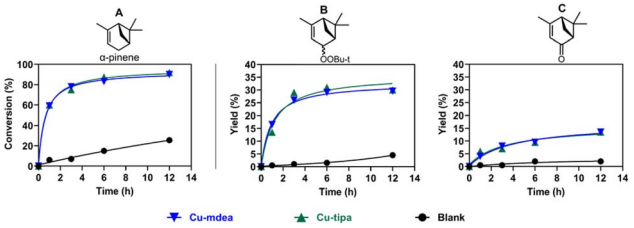

Fig. 4 Cu-catalyzed oxidation of α-pinene with TBHP over **Cu-mdea** (▼) and **Cu-tipa** (▲) (1 mol%) compared to a blank test without Cu^{2+} (●). Conversion of α-pinene (A), accumulation of 4-*tert*-butylperoxy-2-pinene (B) and verbenone (C). Conditions: α-pinene (0.6 mmol), catalyst (6 μmol, **Cu-mdea** and **Cu-tipa**), TBHP (70% in H_2O, 1.2 mmol), CH_3CN (1 mL), 12 h, 1200 rpm, 60 °C, catalytic flask (2 mL).

catalyst (Table S7, ESI†). In polar aprotic solvents, the highest conversion (89%) and total product yield (44%) were achieved in CH_3CN, while in DMSO the respective values are 83% and 33%. However, when using propan-2-ol as a solvent, the conversion of α-pinene decreased significantly to 10.5%, possibly due to competing oxidation of the solvent and/or its binding to the catalyst.[68] These experimental data offer evidence that the reaction is more efficient in aprotic solvents with a relatively high dielectric constant (Table S7, ESI†).

Considering the essential role of catalyst loading in influencing the conversion rate, the catalytic activity of **Cu-mdea** was investigated by varying its concentration from 0.5 to 3 mol%. Fig. 5 and Table S8 (ESI)† illustrate the conversion of α-pinene (84% after 5 h) in a catalytic system comprising 1.5 mol% **Cu-mdea**. In contrast, a 3.0 mol% loading of the catalyst led to the highest substrate conversion (93%, Fig. 5A). Regarding the product yield, at 3.0 mol% **Cu-mdea**, an 18.5% yield of verbenone can be obtained after 5 h, which is higher than that for the reactions carried out with 0.5 mol% and 1.5 mol% catalyst loading (11.5 and 14.5% yields, respectively; Fig. 5C). For 4-*tert*-butylperoxy-2-pinene, the initial rate increased proportionally to catalyst quantity, leading to the most expressive yield of 42% at 3.0 mol% of **Cu-mdea** (Fig. 5B).

Based on these experimental data, the correlation observed between the quantity of catalyst and the enhanced conversion rates can be related to the enhanced availability of active sites. This assumption suggests that a higher number of active sites does not interfere with the diffusion of the reaction products. However, any increase in the conversion beyond the optimal catalyst quantity would yield only modest benefits within a 9 h timeframe. In addition, during the catalytic tests, the results were well reproducible, with the conversion values of α-pinene and product yields following the expected trends. Once the products are formed, they need to diffuse away from the catalyst surface to make room for the adsorption of new reactants. Consequently, the rate of product diffusion can impact the overall reaction rate and efficiency of the catalyst.[69,70] The conversions remain unaffected by the reaction conditions, indicating that the bulk of the 2D CPs is possibly a mesoporous material. Therefore, the product diffusion process is unlikely to be a limiting factor for the conversion values in this catalytic system.

The proposed mechanistic pathway begins with the Cu(II)-mediated conversion of TBHP into a *t*-butoxy radical (t-BuO$^{\bullet}$) and *t*-butyl peroxy radical (t-BuOO$^{\bullet}$).[71,72] The *t*-BuOO$^{\bullet}$ radicals can facilitate not only the generation of alkyl radicals through hydrogen atom abstraction,[73] but also their coordination to a copper(II) center, leading to the formation of active copper-based peroxyl species.[74] These species may participate in the allylic peroxidation of α-pinene by introducing the peroxyl group at 4-position.[75] Subsequently, the homolytic cleavage of the peroxyl group can result in the formation of verbenone, as illustrated in Scheme 2.[73]

The proposed mechanism can be experimentally supported by employing TEMPO ((2,2,6,6-tetramethylpiperidin-1-yl)oxyl) in a Cu-catalyzed oxidation of α-pinene. TEMPO reacts with *t*-BuOO$^{\bullet}$ to catalyze the formation of dioxygen and *t*-BuO$^{\bullet}$ (Scheme S2, ESI†).[76] Hence, in the absence of *t*-BuOO$^{\bullet}$, there is no allylic peroxidation of α-pinene, as attested by a low yield of 4-*tert*-butylperoxy-2-pinene (2% after 6 h). In contrast, verbenone is obtained in a 19% yield (Fig. S18, ESI†), which is slightly higher than that under standard conditions (15%). Besides the homolytic cleavage of the peroxyl group, verbenone may also be formed in a radical system in the presence of O_2,[77] as promoted by the addition of TEMPO to the system (Scheme S2, ESI†).

The allylic peroxidation of the α-pinene was also validated by isolating 4-*tert*-butylperoxy-2-pinene from the reaction over **Cu-**

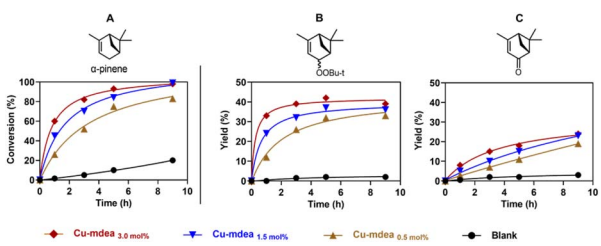

Fig. 5 Cu-catalyzed oxidation of α-pinene with TBHP over **Cu-mdea** (ranging from 0.5 mol% to 3.0 mol%) and a blank test without Cu^{2+}. Conversion of α-pinene (A). Accumulation of 4-*tert*-butylperoxy-2-pinene (B) and verbenone (C). Conditions: α-pinene (0.6 mmol), **Cu-mdea** (0.5–3.0 mol%), TBHP 70% in H_2O (1.2 mmol), CH_3CN (1 mL), 9 h, 1200 rpm, 60 °C, catalytic flask (2 mL).

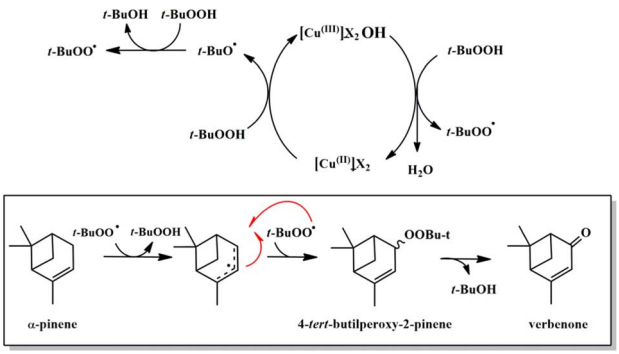

Scheme 2 Mechanistic proposal for the allylic oxidation of α-pinene over a Cu-based catalyst with TBHP as oxidant.

mdea (1 mol%). This elucidation was explored by NMR spectroscopy (^{1}H, ^{13}C, 2D HSQC and ^{1}H-NOESY) in accordance with the literature data (Fig. S19–S22, ESI†).[73]

Temperature-dependent catalytic studies

In order to optimize the reaction conditions, a temperature-dependent study was conducted to investigate the oxidation of α-pinene using 1 mol% of **Cu-dmea** and **Cu-tipa**, with the reaction temperatures ranging from 40 to 80 °C. Fig. S28 (ESI)† presents an overview of this study, highlighting a similar catalytic behavior of both compounds at higher temperatures. From 60 to 80 °C, there is a 92% conversion of α-pinene into 4-*tert*-butylperoxy-2-pinene (32% yield) and verbenone (17% yield) after 12 h. Under these conditions, there is a noticeable increase in the initial reaction rate, as indicated by the upward trend in substrate conversion and the formation of the allylic peroxidation product. Another intriguing correlation is the variation in the ratio of 4-*tert*-butylperoxy-2-pinene (B) to verbenone (C) at different temperatures. At 80 °C, the yields of products B and C were 17 and 32%, respectively, resulting in a B : C molar ratio of 1.9. Conversely, when the reaction is performed at 40 °C, B and C are formed in 5% and 16% yields, respectively (B : C molar ratio of 1 : 3.2). This finding suggests that higher temperatures promote the conversion of reaction intermediates into verbenone. Furthermore, at lower temperatures (40, 50, and 60 °C), the accumulation of pinene epoxides barely surpasses 2%. However, at 70 and 80 °C, pinene epoxides (5.0%) were obtained in the first hour of the reactions. Then, these gradually decompose into products that could not be identified by GC or GC-MS analyses. Fig. S26–S28 and Tables S9–S13 (ESI)† portray the complete temperature-dependent investigation conducted with **Cu-mdea** and **Cu-tipa**.

Hot filtration test and catalyst reusability

To assess the influence of potential leaching of homogeneous species from **Cu-tipa** and **Cu-mdea** in the catalytic system, hot filtration tests were carried out. Their findings were compared to the standard reaction yields and conversions (Fig. 6). The complete hot filtration procedure is described in the ESI.†

The hot filtration test led to a decreased conversion of α-pinene from 92% to 36% after 6 h. This trend was slightly higher than that observed in the blank reaction (Fig. 6A). A similar pattern can be seen in the accumulation of verbenone, reaching the maximum yield of 3.5% (Fig. 6C).

However, an upward trend in the formation of *tert*-butylperoxy-2-pinene was noticeable, reaching 20% after 6 h (Fig. 6). As shown in Fig. S17 (ESI)† and despite the presence of a minor amount of soluble Cu species in the filtrate after the catalyst removal from the reaction medium, the Cu CPs essentially act as heterogeneous catalysts. Additionally, copper content in the reaction solution was analysed by ICP-OES. In fact, only a minor amount of copper (12.6 ppm) leached from **Cu-tipa**, while even a lower leaching (5 ppm) was observed in the system containing **Cu-mdea**. Therefore, both these heterogeneous catalysts are relatively stable during the catalytic process with less than 4% of the copper migrating from the catalyst bulk to the reaction medium.

The efficiency of catalyst recyclability was examined through the successive oxidation of α-pinene using 1 mol% of Cu CPs. The catalysts were reused in consecutive runs without undergoing any pre-treatment, such as thermal or chemical treatment. At the end of each cycle, **Cu-mdea** and **Cu-tipa** were recovered at 96% and 92%, respectively. As indicated in Fig. 7, the catalytic behavior of the recovered compounds closely resembles that of the initially used catalyst.

Cu-mdea maintained its structural integrity throughout the cycles, as confirmed by the powder X-ray diffraction (PXRD) patterns of both the fresh and recovered catalysts (Fig. S30, ESI†). Although **Cu-tipa** also retained its structure during the first three cycles, it exhibited a decline in activity by the fourth run, with the yield of α-pinene oxidation dropping from 41% to 25.5% (Table S14, entry 6, ESI†). This loss of catalytic activity is likely due to partial leaching of metal ions (Fig. S17, ESI†) and structural transformation, as indicated by additional crystallographic phases and the broadening of PXRD bands (Fig. S30, ESI†). In addition, the activity in terms of the TOF values was also sustained over the catalyst recycling, ranging from 13.6 to 12.6 h^{-1} (Fig. 7 and Table S14, entries 1, 2, and 3, ESI†).

Several catalytic systems were explored for verbenone synthesis, particularly through the aerobic oxidation of α-pinene. Among these, a supported Co-polyoxometalate catalyst demonstrated notable performance. For example, Maksimchuk

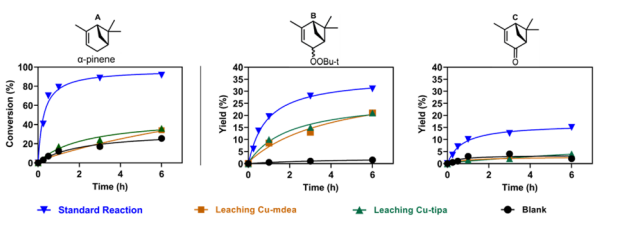

Fig. 6 Hot filtration tests with **Cu-mdea** (■) and **Cu-tipa** (▲) compared to the standard oxidation reaction over **Cu-mdea** (▼). Conversion of α-pinene (A). Accumulation of 4-*tert*-butylperoxy-2-pinene (B) and verbenone (C). Conditions: α-pinene (0.6 mmol), catalyst (1 mol%), TBHP (70% H_2O, 1.2 mmol), CH_3CN (1 mL), 6 h, 1200 rpm, 60 °C, catalytic flask (2 mL).

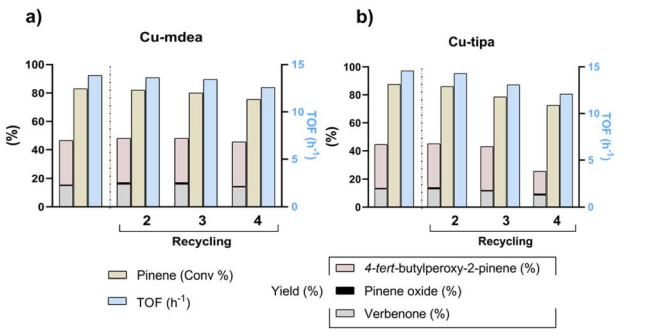

Fig. 7 Recycling test for (a) **Cu-mdea** and (b) **Cu-tipa**. Conditions: α-pinene (0.6 mmol), catalyst (1 mol%), TBHP (70% H_2O, 1.2 mmol), CH_3CN (1 mL), 6 h, 1200 rpm, 60 °C, catalytic flask (2 mL).

et al. achieved a 48% conversion and a maximum verbenone yield of 26% in acetonitrile (50 °C, 1 h).[78] Selvaraj *et al.* reported the high selectivity toward verbenone using a 2D mesoporous chromium silicate catalyst, achieving ~75% conversion with 65% selectivity in chlorobenzene after 9 h.[79] Other notable catalytic systems include a bimetallic $AuCu/TiO_2$ (1/1), which achieved a 94% α-pinene conversion and 65% verbenone selectivity in acetonitrile,[80] and an iron hexadeca chlorinated phthalocyanine on a modified silica, which led to 84% conversion and 23% verbenone selectivity in acetone.[81] In comparison, our study demonstrates superior α-pinene conversion (93%) and good yields of verbenone (25%) along with 4-*tert*-butylperoxy-2-pinene (42%) after 9 h, in addition to using recyclable copper CP catalysts. The present work thus demonstrates distinct advantages over these catalytic systems, not only in terms of verbenone yields but also in using scalable, recoverable, and easily obtainable 2D copper CPs as catalysts.

Regarding the production of 4-*tert*-butylperoxy-2-pinene, the most selective product in this study, only one comparable work was found. This previous study employed a Cu(I) complex in an acetonitrile: acetone system, which led to 85% of α-pinene conversion with 39% yield of 4-*tert*-butylperoxy-2-pinene after 10 days at 0 °C.[75] In contrast, our work demonstrated superior efficiency, resulting in higher α-pinene conversions and product yields after 9 h at 60 °C, under optimized conditions.

Conclusions

In conclusion, this study presents the successful synthesis, scale-up procedure, and structural characterization of two new 2D coordination polymers, **Cu-mdea** and **Cu-tipa**. These were obtained in good yields and under green conditions, using water–ethanol as a reaction medium. The obtained coordination polymers were fully characterized by standard analytical techniques, including FTIR spectroscopy, single and powder X-ray diffraction, and elemental and thermogravimetric analyses. Their structural and topological features were also discussed in detail. Overall, the scale-up process successfully reproduced the **Cu-mdea** and **Cu-tipa** materials on a larger gram scale with improved efficiency and cost-effectiveness. This robust process might be suitable for scaling up the synthesis of similar CPs.

Both coordination polymers act as promising heterogeneous catalysts for the allylic oxidation of α-pinene into value-added oxidation products. The catalysts also revealed reasonable structural stability even after several consecutive runs. **Cu-mdea** and **Cu-tipa** exhibit a relatively similar catalytic behavior under varying temperature-dependent conditions. Under the optimized conditions, the catalytic system comprising **Cu-mdea** can lead to a 93% conversion of α-pinene with the formation of up to 42% of 4-*tert*-butylperoxy-2-pinene and 25% of verbenone. These oxidation products, derived from a low-cost biobased feedstock, can be used as reactive intermediates in organic synthesis.

These findings highlight the potential of the obtained copper(II) compounds as recyclable catalysts for the selective oxidation of α-pinene, making them promising candidates for the development of greener and more sustainable chemical processes. Further research on the design of related catalytic materials and their exploration in the mild oxidative functionalization of terpenes is currently in progress in our laboratories.

Data availability

The data supporting this article have been included as part of the ESI.†

Conflicts of interest

There are no conflicts to declare.

Acknowledgements

This project has received funding from the EU's Horizon 2020 research and innovation programme under Grant Agreement No. 860762 (CHAIR project). We also thank the Foundation for Science and Technology, Portugal (FCT, PTDC/QUI-QIN/3898/2020, UIDB/00100/2020, UIDP/00100/2020, LA/P/0056/2020, and UID/00100/2023). C. H. J. Franco acknowledges the research contracts within the PTDC/QUI-QIN/29697/2017 and PTDC/QUI-QIN/3898/2020 projects (2021–2024). This work was partially carried out by G. Correia at Sorbonne Université (France) and Novartis Pharma (Switzerland) during his secondments within the CHAIR project. The authors also thank Tech. Daniel Naehrig for operational support in the process chemistry laboratory at Novartis Pharma and Dr Tiago Fernandes for assistance with some analyses.

References

1 Y. Jiang, S. Chen, Y. Chen, A. Gu and C. Tang, *J. Am. Chem. Soc.*, 2024, **146**, 2769–2778.
2 J. H. Docherty, T. M. Lister, G. McArthur, M. T. Findlay, P. Domingo-Legarda, J. Kenyon, S. Choudhary and I. Larrosa, *Chem. Rev.*, 2023, **123**, 7692–7760.
3 A. L. García-Cabeza, R. Marín-Barrios, F. J. Moreno-Dorado, M. J. Ortega, G. M. Massanet and F. M. Guerra, *Org. Lett.*, 2014, **16**, 1598–1601.
4 S. Samadi, H. Arvinnezhad, S. Nazari and S. Majidian, *Top. Curr. Chem.*, 2022, **380**, 20.
5 S. Thurow, L. Abenante, J. M. Anghinoni and E. J. Lenardão, *Curr. Org. Synth.*, 2022, **19**, 331–365.
6 F. Musso, V. Gutierrez, M. Volpe and M. Faraoni, *Lat. Am. Appl. Res.*, 2023, **53**, 287–293.
7 F. Panahi, F. Bauer and B. Breit, *Acc. Chem. Res.*, 2023, **56**, 3676–3693.
8 M. Ke, Z. Liu, K. Zhang, S. Zuo and F. Chen, *Green Synth. Catal.*, 2021, **2**, 228–232.
9 A. N. Venancio, L. Menini, D. N. Maronde, E. V. Gusevskaya and L. A. Parreira, *Mol. Catal.*, 2021, **504**, 111449.
10 P. A. Kawale, N. Shekhar, A. Srivastava and S. Banerjee, *Curr. Org. Chem.*, 2024, **28**, 675–685.
11 K. Tabaru and Y. Obora, *Synlett*, 2024, **35**, 1861–1871.
12 M. dos Santos Costa, A. de Camargo Faria and E. V. Gusevskaya, *Appl. Catal., A*, 2019, **584**, 117171.

13 Y. Wen, J. Zheng, A. H. Evans and Q. Zhang, *Organics*, 2023, **4**, 289–296.
14 J. R. Ludwig and C. S. Schindler, *Chem*, 2017, **2**, 313–316.
15 A. Denicourt-Nowicki, M. Rauchdi, M. Ait Ali and A. Roucoux, *Catalysts*, 2019, **9**, 893.
16 H. Wang, Y. Pei, K. Wang, Y. Zuo, M. Wei, J. Xiong, P. Zhang, Z. Chen, N. Shang, D. Zhong and P. Pei, *Small*, 2023, **19**, 2304863.
17 M. Karuppasamy, B. S. Vachan and V. Sridharan, in *Copper in N-Heterocyclic Chemistry*, ed. A. Srivastava, Elsevier, 2021, ch. 7, pp. 249–288.
18 M. Vafaeezadeh, J. Schaumlöffel, A. Lösch, A. De Cuyper and W. R. Thiel, *ACS Appl. Mater. Interfaces*, 2021, **13**, 33091–33101.
19 L. Wang, N. Ma, N. Wu, X. Wang, J. Xin, D. Wang, J. Lin, X. Li and J. Sun, *ACS Appl. Mater. Interfaces*, 2021, **13**, 25461–25471.
20 F. Fan, L. Zhao, Q. Zeng, L. Zhang, X. Zhang, T. Wang and Y. Fu, *ACS Appl. Mater. Interfaces*, 2023, **15**, 37086–37092.
21 Y. Zan, F. Ben Romdhane, A. Miche, C. Méthivier, J.-M. Krafft, C. Jolivalt and J. Reboul, *ACS Appl. Mater. Interfaces*, 2023, **15**, 38716–38728.
22 J. Lee, O. K. Farha, J. Roberts, K. A. Scheidt, S. T. Nguyen and J. T. Hupp, *Chem. Soc. Rev.*, 2009, **38**, 1450–1459.
23 A. E. Wendlandt, A. M. Suess and S. S. Stahl, *Angew. Chem., Int. Ed.*, 2011, **50**, 11062–11087.
24 A. M. Kirillov, M. V. Kirillova and A. J. L. Pombeiro, in *Adv. Inorg. Chem.*, ed. R. van Eldik and C. D. Hubbard, Academic Press, 2013, ch. 1, vol. 65, pp. 1–31.
25 A. N. Bilyachenko, M. S. Dronova, A. I. Yalymov, F. Lamaty, X. Bantreil, J. Martinez, C. Bizet, L. S. Shul'pina, A. A. Korlyukov, D. E. Arkhipov, M. M. Levitsky, E. S. Shubina, A. M. Kirillov and G. B. Shul'pin, *Chem.–Eur. J.*, 2015, **21**, 8758–8770.
26 E. Loukopoulos, A. Abdul-Sada, G. Csire, C. Kállay, A. Brookfield, G. J. Tizzard, S. J. Coles, I. N. Lykakis and G. E. Kostakis, *Dalton Trans.*, 2018, **47**, 10491–10508.
27 J. Gu, M. Wen, Y. Cai, Z. Shi, A. S. Arol, M. V. Kirillova and A. M. Kirillov, *Inorg. Chem.*, 2019, **58**, 2403–2412.
28 A. Hossain, A. Bhattacharyya and O. Reiser, *Science*, 2019, **364**, eaav9713.
29 I. F. M. Costa, M. V. Kirillova, V. André, T. A. Fernandes and A. M. Kirillov, *Inorg. Chem.*, 2021, **60**, 14491–14503.
30 L. Marais, H. C. M. Vosloo and A. J. Swarts, *Coord. Chem. Rev.*, 2021, **440**, 213958.
31 B. Xu, Q. Xu, Q. Wang, Z. Liu, R. Zhao, D. Li, P. Ma, J. Wang and J. Niu, *Inorg. Chem.*, 2021, **60**, 4792–4799.
32 N. Sakamoto, Y. F. Nishimura, T. Nonaka, M. Ohashi, N. Ishida, K. Kitazumi, Y. Kato, K. Sekizawa, T. Morikawa and T. Arai, *ACS Catal.*, 2020, **10**, 10412–10419.
33 E. I. Śliwa, D. S. Nesterov, M. V. Kirillova, J. Kłak, A. M. Kirillov and P. Smoleński, *Inorg. Chem.*, 2021, **60**, 9631–9644.
34 J. Ai, Y. Zhao and Z. z. Tian, *J. Mol. Struct.*, 2023, **1278**, 134873.
35 Y.-H. Gao, P.-P. Huang, H.-T. Xu, P. Huang, B. Liu, J.-F. Lu and H.-G. Ge, *J. Mol. Struct.*, 2023, **1281**, 135106.
36 Q. Zhang, Y. Wang, Y. Ge, Q. Liu and J.-P. Lang, *Inorg. Chem.*, 2023, **62**, 19080–19086.
37 Z. Chen, K. O. Kirlikovali, L. Shi and O. K. Farha, *Mater. Horiz.*, 2023, **10**, 3257–3268.
38 M. Hosseini and D. M. Pereira, *Pharmaceuticals*, 2023, **16**, 202.
39 M. A. Upshur, A. G. Bé, J. Luo, J. G. Varelas, F. M. Geiger and R. J. Thomson, *Nat. Prod. Rep.*, 2023, **40**, 890–921.
40 N. Semmar, in *Secondary Metabolites in Plant Stress Adaptation: Analytic Space of Secondary Metabolites*, ed. N. Semmar, Springer International Publishing, Cham, 2024, pp. 71–109.
41 M. M. Karimkhani, M. Nasrollahzadeh, M. Maham, A. Jamshidi, M. S. Kharazmi, D. Dehnad and S. M. Jafari, *Crit. Rev. Food Sci. Nutr.*, 2024, **64**, 4286–4311.
42 S. S. P. Dias, M. V. Kirillova, V. André, J. Kłak and A. M. Kirillov, *Inorg. Chem.*, 2015, **54**, 5204–5212.
43 T. A. Fernandes, C. I. M. Santos, V. André, S. S. P. Dias, M. V. Kirillova and A. M. Kirillov, *Catal. Sci. Technol.*, 2016, **6**, 4584–4593.
44 T. A. Fernandes, C. I. M. Santos, V. André, J. Kłak, M. V. Kirillova and A. M. Kirillov, *Inorg. Chem.*, 2016, **55**, 125–135.
45 T. A. Fernandes, V. André, A. M. Kirillov and M. V. Kirillova, *J. Mol. Catal. A: Chem.*, 2017, **426**, 357–367.
46 M. V. Kirillova, P. T. d. Paiva, W. A. Carvalho, D. Mandelli and A. M. Kirillov, *Pure Appl. Chem.*, 2017, **89**, 61–73.
47 M. V. Kirillova, C. I. M. Santos, V. André, T. A. Fernandes, S. S. P. Dias and A. M. Kirillov, *Inorg. Chem. Front.*, 2017, **4**, 968–977.
48 T. A. Fernandes, M. V. Kirillova, V. André and A. M. Kirillov, *Dalton Trans.*, 2018, **47**, 16674–16683.
49 F. M. Scaldini, C. C. Corrêa, M. I. Yoshida, K. Krambrock and F. C. Machado, *J. Coord. Chem.*, 2014, **67**, 2967–2982.
50 X.-W. Liu, R. Guo, H. Liu, Y.-Q. Yu, X.-W. Qi, J.-Y. Xu and C.-Z. Xie, *RSC Adv.*, 2015, **5**, 15059–15068.
51 A. M. Kirillov and G. B. Shul'pin, *Coord. Chem. Rev.*, 2013, **257**, 732–754.
52 Bruker, *Apex 3, V2018. 1–0, SAINT V8. 40B*, Bruker AXS Inc., Madison, 2018.
53 G. Shelx, *Acta Crystallogr.*, 2008, **64**, 112–122.
54 O. V. Dolomanov, L. J. Bourhis, R. J. Gildea, J. A. Howard and H. Puschmann, *J. Appl. Crystallogr.*, 2009, **42**, 339–341.
55 G. Sheldrick, *TWINABS 2012/1*, Georg-August-University Göttingen, Germany, 2012.
56 G. M. Sheldrick, *SHELXL-2018*, Universität Göttingen, Göttingen, Germany, 2018.
57 G. M. Sheldrick, *SHELXL-2018/3 Software Package*, University of Göttingen, Germany, 2018.
58 C. H. J. Franco, W. R. do Carmo, F. B. de Almeida, H. A. de Abreu and R. Diniz, *Struct. Chem.*, 2015, **26**, 773–783.
59 L. Yang, D. R. Powell and R. P. Houser, *Dalton Trans.*, 2007, **9**, 955–964.
60 *Reticular Chemistry Structure Resource*, **http://rcsr.net/**, accessed 01-09-2024.
61 V. A. Blatov, M. O'Keeffe and D. M. Proserpio, *CrystEngComm*, 2010, **12**, 44–48.

62 C. H. J. Franco, P. Chagas, G. S. Caldeira, L. C. A. Oliveira, P. P. de Souza, A. A. Leitão, G. W. Amarante and R. Diniz, *Dalton Trans.*, 2018, **47**, 10976–10988.
63 Y. Ai, W. Li and D. Zhao, *Natl. Sci. Rev.*, 2022, **9**, nwab108.
64 M. M. Karimkhani, M. Nasrollahzadeh, M. Maham, A. Jamshidi, M. S. Kharazmi, D. Dehnad and S. M. Jafari, *Crit. Rev. Food Sci. Nutr.*, 2022, **64**, 4286–4311.
65 F. Roudesly, J. Oble and G. Poli, *J. Mol. Catal. A:Chem.*, 2017, **426**, 275–296.
66 J. Zhang, D. Xiao, H. Tan and W. Liu, *J. Org. Chem.*, 2020, **85**, 3929–3935.
67 Q. Yang, Z. Wang, T. Kato, Y. Liu and K. Maruoka, *Org. Lett.*, 2023, **25**, 2958–2963.
68 S. Yagishita, A. Himegi, K. Kanazashi, T. Ohishi, R. Ishikawa, T. Hamaguchi and S. Kawata, *Dalton Trans.*, 2017, **46**, 2966–2973.
69 B. C. Bukowski, F. A. Son, Y. Chen, L. Robison, T. Islamoglu, R. Q. Snurr and O. K. Farha, *Chem. Mater.*, 2022, **34**, 4134–4141.
70 D. S. Grebenkov, *Molecules*, 2023, **28**, 7570.
71 D. Saberi, F. Shojaeyan and K. Niknam, *Tetrahedron Lett.*, 2016, **57**, 566–569.
72 S. Jyoti, M. Devi, D. Wadhwa, J. Sindhu and V. Kumar, *Eur. J. Org Chem.*, 2024, **27**, e202301030.
73 L. Capaldo and D. Ravelli, *Eur. J. Org Chem.*, 2017, **2017**, 2056–2071.
74 A. Bravo, H.-R. Bjørsvik, F. Fontana, L. Liguori and F. Minisci, *J. Org. Chem.*, 1997, **62**, 3849–3857.
75 M. Schulz, R. Kluge and F. Gadissa Gelalcha, *Tetrahedron:Asymmetry*, 1998, **9**, 4341–4360.
76 D. H. R. Barton, V. N. Le Gloahec and J. Smith, *Tetrahedron Lett.*, 1998, **39**, 7483–7486.
77 U. Neuenschwander, F. Guignard and I. Hermans, *ChemSusChem*, 2010, **3**, 75–84.
78 N. Maksimchuk, M. Melgunov, Y. A. Chesalov, J. Mrowiec-Białoń, A. Jarzębski and O. Kholdeeva, *J. Catal.*, 2007, **246**, 241–248.
79 M. Selvaraj, M. Kandaswamy, D. Park and C. Ha, *Catal. Today*, 2010, **158**, 286–295.
80 S. Ajaikumar, J. Ahlkvist, W. Larsson, A. Shchukarev, A.-R. Leino, K. Kordas and J.-P. Mikkola, *Appl. Catal., A*, 2011, **392**, 11–18.
81 J.-A. Becerra, L.-M. González and A.-L. Villa, *J. Mol. Catal. A: Chem.*, 2016, **423**, 12–21.